

Warm Surprises from Cold Duets: N-Body Simulations with Two-Component Dark Matter

Jeong Han Kim,^{1,*} Kyoungchul Kong,^{2,†} Se Hwan Lim,^{1,‡} and Jong-Chul Park^{3,§}

¹*Department of Physics, Chungbuk National University, Cheongju, Chungbuk 28644, Republic of Korea*

²*Department of Physics and Astronomy, University of Kansas, Lawrence, KS 66045, USA*

³*Department of Physics and IQS, Chungnam National University, Daejeon 34134, Republic of Korea*

We explore extensive N -body simulations with two-component cold dark matter candidates. We delve into the temperature evolution, power spectrum, density perturbation, and maximum circular velocity functions. We find that the substantial mass difference between the two candidates and the annihilation of the heavier components to the lighter ones effectively endow the latter with warm dark matter-like behavior, taking advantage of all distinct features that warm dark matter candidates offer, without observational bounds on the warm dark matter mass. Moreover, we demonstrate that the two-component dark matter model aligns well with observational data, providing valuable insights into where and how to search for the elusive dark matter candidates in terrestrial experiments.

Introduction. Nature of dark matter (DM) remains mysterious even after decades of a multitude of experiments in particle physics and great advances in observational astrophysics and cosmology [1]. The majority of cosmological simulations focus on a single DM candidate for its simplicity and approximate consistency with much of observational data, while various theoretical models of dark matter, including multi-component dark matter [2, 3], have been proposed to address some of unresolved queries and to better understand data in current and upcoming experiments [4]. Most existing studies on two-component dark matter consider N -body simulation with non-interacting two cold dark matter (CDM) components [5] or with non-interacting CDM and warm dark matter (WDM) [6–10]. A non-trivial connection between two-component dark matters and its cosmology has been discussed in literature, but the model requires extremely degenerate mass spectrum $\Delta m/m \sim 10^{-8}$ [11–15].

In this paper, we go beyond one single CDM paradigm and perform comprehensive cosmological simulations for two-component CDM candidates with the sizable mass splitting and self-interaction (diagram II in Figure 1) for the light component. After both components decouple from the thermal bath, in addition to the heavy CDM, we expect two types of light CDMs to arise: relic (non-relativistic) component and boosted DM from the annihilation of the heavy CDM. The light-boosted components share their energy with the slow-relic component, increasing the temperature via sizable non-gravitational self-interaction, and therefore making the light relic behave like WDM, as illustrated in Figure 1. Such a scenario naturally connects between models with two CDMs and models with CDM + WDM. Therefore, this model innately takes advantage of all distinct features that WDM

offers, such as power spectrum, dark matter density profile, small-scale structures, etc. On the other hand, it suffers less from observational bounds on the WDM mass. For example, WDM mass bound from Lyman- α observation [16, 17] is significantly weakened or negligible in this model. WDM becomes hotter as it gets lighter. However, our model controls such behavior with the relic fraction of the light component to the total DM abundance and mass splitting.

Many direct detection schemes have been proposed targeting sub-MeV DM [18–23], while currently operating experiments are not sensitive to the typical WDM mass [24, 25]. However, the boosted property of the light DM component offers great opportunity in the particle physics experiments [26–54] and cosmological thermal dynamics [55]. Yet, little studies on cosmological implications of such boosted DM models have been discussed. In this paper, we will carefully examine the temperature evolution, density perturbation, and N -body simulation of the two-component DM model. We derive the model parameters that are consistent with the maximum circular velocity function (MCVF), which can be studied in current and upcoming particle physics experiments.

Model. We consider a two-component DM model with a dark sector consisting of two Dirac fermions χ_1 and χ_2 with mass hierarchy $m_2 > m_1$, whose stability is protected by dark $U(1)' \otimes U(1)''$ gauge symmetries [3]. We assume that both χ_1 and χ_2 are charged under $U(1)''$, while only χ_1 is charged under $U(1)'$. The dark sector is allowed to couple to the standard model (SM) sector only through a kinetic mixing between $U(1)'$ and $U(1)_Y$. The dark gauge symmetries are assumed to be spontaneously broken, leading to the dark gauge boson masses $m_{A'}$ and $m_{A''}$, respectively. We are interested in the scenario where dark gauge bosons are heavier than χ_1 and χ_2 . In this case, χ_2 is disjunct from the SM particles and annihilates only into the other DM species χ_1 , while χ_1 can directly annihilate into the SM particles.

The heavy species χ_2 is kept to thermal equilibrium by the assist of the light species χ_1 [3] with a thermally-

*Electronic address: jeonghan.kim@cbu.ac.kr

†Electronic address: kckong@ku.edu

‡Electronic address: sehwan.lim@chungbuk.ac.kr

§Electronic address: jcpark@cnu.ac.kr

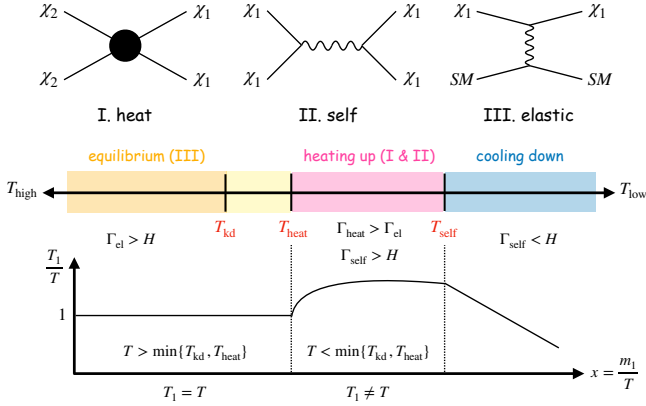


FIG. 1: Brief thermal history of the universe with two-component CDMs. Different stages are defined by three important temperatures, T_{kd} , T_{heat} , and T_{self} , which are determined by the balance between the various interaction rates and the Hubble parameter H : $\Gamma_{el} \leftrightarrow H$, $\Gamma_{el} \leftrightarrow \Gamma_{heat}$, and $\Gamma_{self} \leftrightarrow H$, respectively. Γ_{heat} , Γ_{self} , and Γ_{el} are the interaction rates due to heating process (I), self-interaction (II), and elastic scattering (III), respectively.

averaged annihilation cross section $\langle\sigma v\rangle_{22\rightarrow 11}$, while χ_1 pair-annihilates directly to SM particles with the cross section $\langle\sigma v\rangle_{11\rightarrow XX}$ where X stands for SM particles. We assume χ_1 couples to electrons predominantly, for simplicity. Relic abundances of χ_1 and χ_2 denoted as Ω_1 and Ω_2 respectively, and the total abundance should agree with the observed one, $\Omega_{DM} = \Omega_1 + \Omega_2 \simeq 0.27$. The fraction of χ_1 is expressed by $r_1 = \Omega_1/\Omega_{DM}$. The free parameters of the model are $\{m_1, m_2, m_{A'}, m_{A''}, g', g'', \epsilon\}$, where g' and g'' denote gauge couplings for $U(1)'$ and $U(1)''$ respectively, and ϵ is the kinetic mixing parameter between $U(1)'$ and $U(1)_Y$. In this paper, we will mainly focus on cosmological features of the model. Thus, the parameters can be traded with relevant effective parameters $\{m_1, m_2, \Omega_{DM}, r_1, \sigma_{self1}, \sigma_{self2}\}$, where Ω_{DM} is fixed by 0.27 to yield the observed value and σ_{self1} (σ_{self2}) denotes a self-scattering cross section of χ_1 (χ_2). We note that σ_{self1} (diagram II in Figure 1) plays an important role in sharing the excessive kinetic energy of boosted χ_1 particles with the rest of their species and hence increase the overall χ_1 temperature $T_1 = T_{\chi_1}$ [55]. In principle, the self-interaction of non-relativistic χ_2 particles can also influence on perturbation evolution, but to focus on the main dynamics of χ_1 self-heating, we will neglect the contribution of σ_{self2} in our discussions. Therefore, the parameters determining the most prominent features in cosmological simulation are $\{m_1, m_2, r_1, \sigma_{self1}\}$.

Temperature evolution. Cosmological evolution for the number densities of χ_1 , χ_2 , and SM particles X , $n_{1,2,X}$ are governed by coupled Boltzmann equations as in Refs. [3, 55], and will be discussed with details in a companion paper [56]. Here, we focus on the temperature evolution of the light component χ_1 .

After the decoupling of DM particles from the SM

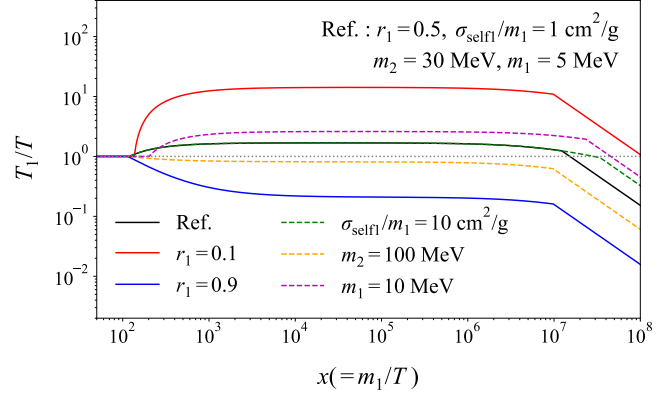


FIG. 2: Temperature evolution T_1 of dark matter χ_1 as a function of $x = m_1/T$ under various benchmark model parameters.

plasma (with temperature T), the $\bar{\chi}_2\chi_2 \rightarrow \bar{\chi}_1\chi_1$ annihilation (diagram I in Figure 1) can leverage the mass gap $\delta m = m_2 - m_1$ to produce energetic χ_1 particles. If $\Gamma_{self} > H$, the excessive kinetic energy ($\Gamma_{heat} > \Gamma_{el}$) is thermalized to increase the overall temperature of χ_1 particles (heating up period in Figure 1). The evolution of its temperature T_1 is governed by

$$\dot{T}_1 \simeq -2HT_1 + \gamma_{heat}T - 2\gamma_{\chi_1 X}(T_1 - T), \quad (1)$$

where the first term on the right-hand side represents the Hubble friction due to the expansion of the Universe, and the second is responsible for the self-heating with $\gamma_{heat} \simeq 2n_2^2\langle\sigma v\rangle_{22\rightarrow 11}\delta m/(3n_1T)$ [55]. Note that although the larger mass difference δm leads to the higher temperature T_1 in general, it is closely associated with the relative number densities of χ_1 and χ_2 as well. The last term of Eq. (1) describes the energy exchange between χ_1 and the SM plasma with $\gamma_{\chi_1 X} \simeq (\delta E/T)n_X\langle\sigma v\rangle_{\chi_1 X}$, where δE is the change in χ_1 kinetic energy per elastic scattering and $\langle\sigma v\rangle_{\chi_1 X}$ is the thermally averaged scattering cross section of χ_1 off SM particles [55].

Figure 2 shows the evolution of T_1/T as a function of $x = m_1/T$ for a few selections of parameter sets by varying one parameter at a time with respect to a benchmark point ($r_1 = 0.5$, $\sigma_{self1}/m_1 = 1 \text{ cm}^2/\text{g}$, $m_2 = 30 \text{ MeV}$, $m_1 = 5 \text{ MeV}$). Results in Figure 2 are exactly what was expected from the illustration in Figure 1. Several important comments are in order. First, to boost the temperature T_1 , a larger χ_2 density is favored ($r_1 \ll 1$). On the other hand, if the χ_2 density is smaller than χ_1 ($r_1 \rightarrow 1$), less amount of energetic χ_1 particles are produced from the χ_2 annihilation. With only a small amount of extra energy available, it is not enough to heat a large portion of the relic χ_1 population, which leads to a lower T_1 temperature. Second, the self-interaction σ_{self1}/m_1 determines the duration of the self-heating effect. For example, with an increase in σ_{self1}/m_1 from $1 \text{ cm}^2/\text{g}$ (black solid) to $10 \text{ cm}^2/\text{g}$ (green dashed), the more prolonged time that T_1 is heated, and hence its temperature starts

to fall much later. Finally, the self-heating is more sensitive to the combination of number density n_2^2/n_1 than the mass difference δm . An increase of m_2 from 30 MeV (black solid) to 100 MeV (orange dashed) leads to a large δm , but the number density n_2 drops as $n_2 \simeq \rho_2/m_2$ for non-relativistic particles. As a result, T_1 of the $m_2 = 100$ MeV case is lower than the $m_2 = 30$ MeV case. Similarly, an increase of m_1 from 5 MeV (black solid) to 10 MeV (purple dashed) leads to a larger temperature due to the decreased number density n_1 .

Perturbation evolution. We are now ready to derive the matter perturbation equations. We focus on the perturbations of χ_1 and χ_2 fluids, while investigating the

perturbations of SM fluids is left for future works [56]. We introduce the metric fluctuations in the Newtonian gauge as

$$ds^2 = -(1 + 2\Psi)dt^2 + (1 - 2\Phi)a(t)^2\delta_{ij}dx^i dx^j, \quad (2)$$

where $a(t)$ is a cosmological scale factor, Ψ and Φ denote scalar perturbations. Manipulating the standard procedure with the metric fluctuations and covariant derivatives of energy-momentum tensors [57], we derive the following coupled differential equations for the density perturbation (for the first time):

$$\frac{d\delta_2}{dt} + \frac{\theta_2}{a} - 3\frac{d\Phi}{dt} = \frac{\langle\sigma v\rangle_{22\rightarrow 11}}{m_2\bar{\rho}_2} \left(-\Psi\left(\bar{\rho}_2^2 - \frac{\bar{\rho}_{2,\text{eq}}^2}{\bar{\rho}_{1,\text{eq}}^2}\bar{\rho}_1^2\right) - \bar{\rho}_2^2\delta_2 + \frac{\bar{\rho}_{2,\text{eq}}^2}{\bar{\rho}_{1,\text{eq}}^2}\bar{\rho}_1^2(2\delta_{2,\text{eq}} - \delta_2 - 2\delta_{1,\text{eq}} + 2\delta_1) \right), \quad (3)$$

$$\frac{d\theta_2}{dt} + H\theta_2 + \frac{\nabla^2\Psi}{a} = \frac{\langle\sigma v\rangle_{22\rightarrow 11}}{m_2\bar{\rho}_2} \frac{\bar{\rho}_{2,\text{eq}}^2}{\bar{\rho}_{1,\text{eq}}^2}\bar{\rho}_1^2(\theta_1 - \theta_2), \quad (4)$$

$$\begin{aligned} \frac{d\delta_1}{dt} + \frac{\theta_1}{a} - 3\frac{d\Phi}{dt} &= -\frac{\langle\sigma v\rangle_{22\rightarrow 11}}{m_2\bar{\rho}_1} \left(-\Psi\left(\bar{\rho}_2^2 - \frac{\bar{\rho}_{2,\text{eq}}^2}{\bar{\rho}_{1,\text{eq}}^2}\bar{\rho}_1^2\right) - \bar{\rho}_2^2(2\delta_2 - \delta_1) + \frac{\bar{\rho}_{2,\text{eq}}^2}{\bar{\rho}_{1,\text{eq}}^2}\bar{\rho}_1^2(2\delta_{2,\text{eq}} + \delta_1 - 2\delta_{1,\text{eq}}) \right) \\ &+ \frac{\langle\sigma v\rangle_{11\rightarrow XX}}{m_1\bar{\rho}_1} \left(-\Psi\left(\bar{\rho}_1^2 - \bar{\rho}_{1,\text{eq}}^2\right) - \bar{\rho}_1^2\delta_1 + \bar{\rho}_{1,\text{eq}}(2\delta_{1,\text{eq}} - \delta_1) \right), \end{aligned} \quad (5)$$

$$\frac{d\theta_1}{dt} + H\theta_1 + \frac{\nabla^2\Psi}{a} + c_{s,1}^2 \frac{\nabla^2\delta_1}{a} = \frac{\langle\sigma v\rangle_{22\rightarrow 11}}{m_2\bar{\rho}_1} \bar{\rho}_2^2(\theta_2 - \theta_1), \quad (6)$$

where ρ_α , $\bar{\rho}_\alpha$, $\delta_\alpha = \delta\rho_\alpha/\bar{\rho}_\alpha$, and θ_α represent energy densities, background energy densities, density contrasts, and velocity divergence fields, respectively.

Eqs. (3–6) reproduce the perturbed Boltzmann equations for the CDMs in the vanishing non-gravitational interaction limit. The source terms on the right-hand side of Euler equations in Eqs. (4, 6) describe the momentum transfers between the χ_2 and χ_1 particles which are proportional to the scattering rate, $\langle\sigma v\rangle_{22\rightarrow 11}$ and to the difference in χ_2 and χ_1 velocities, $\theta_2 - \theta_1$. As expected, the scattering tries to make the χ_1 particles move faster for large $\langle\sigma v\rangle_{22\rightarrow 11}$. The last term on the left-hand side of Eq. (6) describes the pressure of χ_1 DM as a consequence of the temperature increase from the self-heating effect. The sound speed of χ_1 fluid is computed from

$$c_{s,1}^2 = \frac{T_1}{m_1} \left(1 - \frac{1}{3} \frac{\partial \ln T_1}{\partial \ln a} \right), \quad (7)$$

where we have used Eq. (1) for T_1 . On the other hand, since the χ_2 particles behave like pressureless CDM, we neglect the pressure term for χ_2 in our analysis. Finally, the evolution of gravity perturbations, Ψ and Φ , are governed by the space-time and space-space components of perturbed Einstein equations. In the pres-

ence of the anisotropic tensors due to the contributions from photons and neutrinos, in general $\Psi \neq \Phi$, which we consider properly in our study. We follow the calculation using two density contrasts in the multi-interacting DM scenario [58] with CLASS [59]. We use the following parameters based on Planck 2018 [60] Λ CDM parameters, $\{\Omega_\Lambda, \Omega_m, \Omega_b, h, \sigma_8\} = \{0.6889, 0.3111, 0.049, 0.6766, 0.8102\}$ for the analysis in the rest of this paper.

Figure 3 shows the evolution of density contrasts δ_1 (dashed) and δ_2 (solid) as a function of a scale factor a for a fixed mode $k = 50 \text{ Mpc}^{-1}$. The δ_2 goes through a significant change around the time of matter-radiation equality, $a \sim \mathcal{O}(10^{-4})$. In the single-component DM limit of $r_1 \simeq 0$, the matter energy density is dominated by χ_2 , and the evolution of δ_2 resembles that of the single CDM model. This picture starts to deviate as the r_1 increases, where the annihilation cross section $\langle\sigma v\rangle_{22\rightarrow 11}$ becomes large. It turns out that in this case the δ_2 experiences a stronger friction due to the disappearance of the gravitational potential well from the χ_2 annihilation, and hence its overall growth is suppressed.

The δ_1 exhibits the oscillatory behavior which hinders the growth of matter perturbations, even in the deep radiation era. In the limit $r_1 \simeq 0$, the annihilation cross

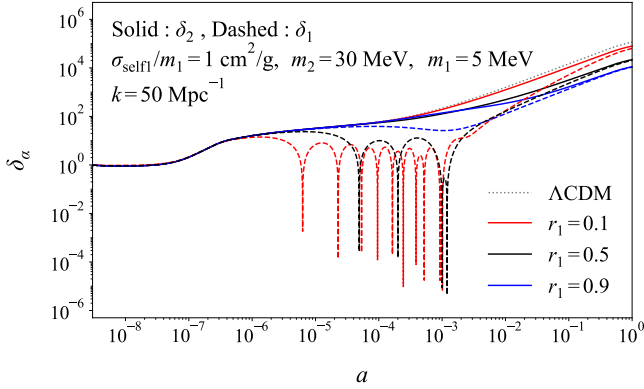


FIG. 3: Evolution of dark matter density perturbations under various benchmark model parameters.

section $\langle\sigma v\rangle_{22\rightarrow 11}$ becomes small, which leads to a shallow gravitational potential well of χ_1 . In this case, the pressure from the self-heating effect dominates over the gravity, causing the oscillatory behavior. However, as r_1 increases, the gravity becomes a match-fit with the pressure, and at some point δ_1 stops oscillating.

All the features described above are somewhat less significant for a small k mode. The evolution of δ_2 is nearly the same as that of CDM and unaffected by the ratio parameter r_1 . There is a slight suppression in δ_1 in the limit $r_1 \ll 1$, but it does not show the oscillatory behavior.

Linear power spectrum. With the density perturbations δ_1 and δ_2 obtained above, the linear matter power spectrum can be readily computed with CLASS [59], as shown in Figure 4. In the WDM scenarios, the particles are in a relativistic state during the deep radiation epoch, which causes the density perturbations of the particles to be suppressed at the scale below free-streaming length. Analogously, in the multi-component model, the power spectrum is suppressed as a result of the self-heating effect through self-interaction of χ_1 . Therefore, the CDM candidate χ_1 at the MeV mass scale behaves like WDM (at the keV mass scale) via the interactions between dark matter particles. Similarly, the oscillatory behavior at $k \gtrsim 100 h/\text{Mpc}$ (often known as the characteristic of the WDMs) is due to the competition between the gravitational potential and the pressure of the χ_1 fluid.

The suppression scale k depends on r_1 . For $k < 20 h/\text{Mpc}$, the suppression becomes maximal at an intermediate value of r_1 , and then the power spectrum increases toward the ΛCDM case, as r_1 increases: e.g., $r_1 \sim 0.5$ leads to the lowest power spectrum below $k \sim 20 h/\text{Mpc}$ for the reference choice in Figure 4. On the other hand, for $k > 100 h/\text{Mpc}$, the larger r_1 leads to the lower power spectrum because there are too many χ_1 particles with self-interaction in the large r_1 limit.

Note that the elastic scattering between χ_1 and χ_2 , and that between χ_1 and photons contribute to the right-hand side of Eq. (4) and Eq. (6), respectively. The χ_1 -photon elastic scattering suppresses the power spectrum

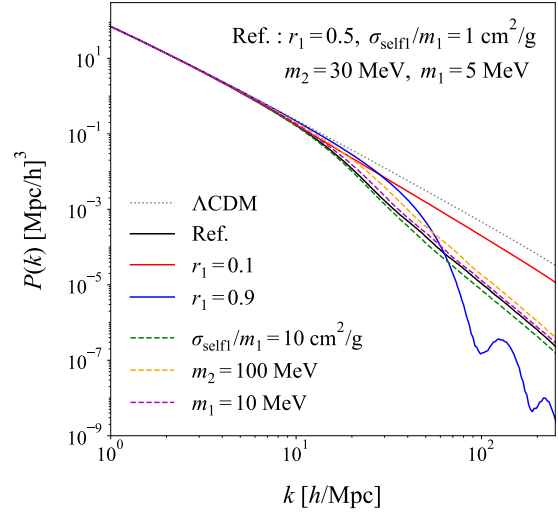


FIG. 4: Linear matter power spectrum for various choices of parameters.

as the χ_1 perturbations are suppressed on scales that enter the horizon before the kinetic decoupling [61, 62]. Such effects appear at $k \gtrsim 500 h/\text{Mpc}$ for a large value of r_1 in our power spectrum, which we find negligible.

N-body simulation. We perform N -body simulations using two-component DM simulation [12] built on GADGET-3 [63, 64] to investigate the non-linear effects. We use a periodic comoving box with the size $3 h^{-1}\text{Mpc}$ and the total number of particles 128^3 . All simulations are carried to the redshift $z_f = 0$ with the initial redshift $z_i = 49$. We adopt 2LPTIC [65] for the second-order Lagrangian perturbation theory to generate initial conditions with the linear matter power spectrum as inputs (obtained from CLASS). In N -body simulations with WDM [66–68] or mixed CDM-WDM [6–10], the thermal velocity is additionally considered in the Zel’dovich velocity to take into account the thermal effect of WDM particles. However, in our simulation, the masses of two particles are large enough compared to WDM (in our model, $m_{1,2} \geq 5 \text{ MeV}$), and therefore such thermal effects are negligible.

We extract halo and sub-halo catalogs using Friends-Of-Friends (FOF) halo finder and SUBFIND [69] algorithms in GADGET-4 [70]. Among many interesting quantities, we focus on the maximum velocity of sub-halos, i.e., MCVF, which is related to the mass scale of the sub-halos. Figure 5 shows the number of accumulated sub-halos ($N(> V_{\text{max}})$) as a function of their maximum velocity (V_{max}) for various selections of parameters with respect to the reference. The larger value of V_{max} implies the heavier sub-halos. Our results show that in the multi-component scenario, the number of sub-halos is reduced compared to ΛCDM simulation, mitigating the so-called missing satellite problem [71, 72]. Baryonic effects are also known to lower the magnitude of MCVF [73, 74]. However, such effects may not be strong enough for ex-

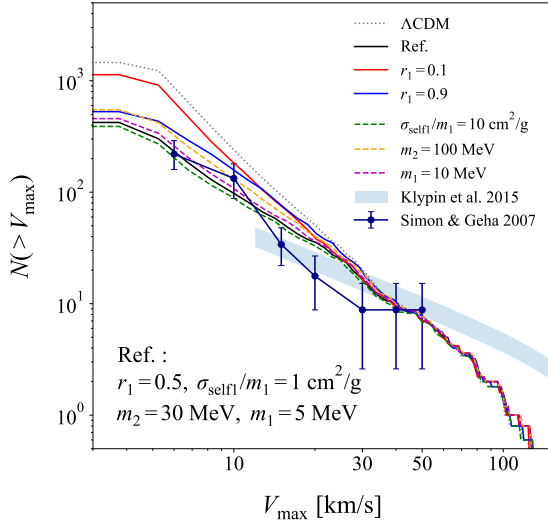


FIG. 5: The number of accumulated sub-halos as a function of the maximum circular velocity for various parameters in the two-component dark matter model.

perimental data, which motivates the inclusion of WDM additionally [73, 74]. Our two-component dark matters are similar in the sense that the light CDM component plays a role of WDM in N -body simulation.

Conclusion and outlook. In this paper, we introduced a model with two-component CDM, where the lighter one behaves like WDM. For the first time, we have investigated the temperature evolution, density perturbation, linear power spectrum, and maximum circular velocity function via N -body simulation. Such various cosmological implications provide a crucial input to particle physics experiments. For example, performing a simple fit to the MCVF in Figure 5 returns a benchmark reference model, with which one can compute the expected event rates (via the elastic scattering process III in Figure 1) per year at terrestrial experiments such as Super-Kamiokande [75], XENONnT [76], and JUNO [77]. Further discussion is needed for the full investigation of cosmological and phenomenological implications of boosted dark matter, including nonlinear power spectrum, halo profile, baryonic effect, and gravitational wave signals, which is beyond the scope of the current study and will be performed somewhere else [56].

Acknowledgments. We thank Donghui Jeong, Jinn-Ouk Gong and Chang Sub Shin for useful discussion. The work is supported by the National Research Foundation of Korea (NRF) [NRF-2021R1C1C1005076 (JHK, SHL), NRF-2019R1C1C1005073 (JCP)]. KK is supported in part by US DOE DE-SC0024407 and University of Kansas General Research Fund allocation.

-
- [1] J. Cooley et al. (2022), 2209.07426.
 - [2] F. D’Eramo and J. Thaler, JHEP **06**, 109 (2010), 1003.5912.
 - [3] G. Belanger and J.-C. Park, JCAP **03**, 038 (2012), 1112.4491.
 - [4] L. Perivolaropoulos and F. Skara, New Astron. Rev. **95**, 101659 (2022), 2105.05208.
 - [5] H. Huang, H.-Y. Schive, and T. Chiueh, Mon. Not. Roy. Astron. Soc. **522**, 515 (2023), 2212.14288.
 - [6] A. V. Maccio, O. Ruchayskiy, A. Boyarsky, and J. C. Muñoz-Cuartas, Mon. Not. Roy. Astron. Soc. **428**, 882 (2013), 1202.2858.
 - [7] G. Parimbelli, G. Scelfo, S. K. Giri, A. Schneider, M. Archidiacono, S. Camera, and M. Viel, JCAP **12**, 044 (2021), 2106.04588.
 - [8] A. Boyarsky, J. Lesgourgues, O. Ruchayskiy, and M. Viel, Journal of Cosmology and Astroparticle Physics **2009**, 012 (2009), URL <https://doi.org/10.1088/2F1475-7516/2F2009/2F05/2F012>.
 - [9] A. V. Maccio, O. Ruchayskiy, A. Boyarsky, and J. C. Muñoz-Cuartas, Monthly Notices of the Royal Astronomical Society **428**, 882 (2012), URL <https://doi.org/10.1093/Fmnras/2Fsts078>.
 - [10] D. Anderhalden, J. Diemand, G. Bertone, A. Maccio, and A. Schneider, Journal of Cosmology and Astroparticle Physics **2012**, 047 (2012), URL <https://doi.org/10.1088/2F1475-7516/2F2012/2F10/2F047>.
 - [11] M. V. Medvedev, Phys. Rev. Lett. **113**, 071303 (2014), 1305.1307.
 - [12] K. Todoroki and M. V. Medvedev, Monthly Notices of the Royal Astronomical Society **483**, 3983 (2018), URL <https://doi.org/10.1093/Fmnras/2Fsty3401>.
 - [13] K. Todoroki and M. V. Medvedev, Mon. Not. Roy. Astron. Soc. **483**, 3983 (2019), 1711.11078.
 - [14] K. Todoroki and M. V. Medvedev, Mon. Not. Roy. Astron. Soc. **483**, 4004 (2019), 1711.11085.
 - [15] K. Todoroki and M. V. Medvedev, Mon. Not. Roy. Astron. Soc. **510**, 4249 (2022), 2003.11096.
 - [16] A. Garzilli, A. Magalich, O. Ruchayskiy, and A. Boyarsky, Mon. Not. Roy. Astron. Soc. **502**, 2356 (2021), 1912.09397.
 - [17] B. Villaseñor, B. Robertson, P. Madau, and E. Schneider, Phys. Rev. D **108**, 023502 (2023), 2209.14220.
 - [18] Y. Hochberg, Y. Zhao, and K. M. Zurek, Phys. Rev. Lett. **116**, 011301 (2016), 1504.07237.
 - [19] K. Schutz and K. M. Zurek, Phys. Rev. Lett. **117**, 121302 (2016), 1604.08206.
 - [20] Y. Hochberg, Y. Kahn, M. Lisanti, K. M. Zurek, A. G. Grushin, R. Ilan, S. M. Griffin, Z.-F. Liu, S. F. Weber, and J. B. Neaton, Phys. Rev. D **97**, 015004 (2018), 1708.08929.
 - [21] S. Knapen, T. Lin, M. Pyle, and K. M. Zurek, Phys. Lett. B **785**, 386 (2018), 1712.06598.
 - [22] Y. Hochberg, I. Charaev, S.-W. Nam, V. Verma, M. Colangelo, and K. K. Berggren, Phys. Rev. Lett. **123**, 151802 (2019), 1903.05101.
 - [23] D. Kim, J.-C. Park, K. C. Fong, and G.-H. Lee (2020), 2002.07821.
 - [24] L. Barak et al. (SENSEI), Phys. Rev. Lett. **125**, 171802 (2020), 2004.11378.

- [25] Y. Hochberg, B. V. Lehmann, I. Charaev, J. Chiles, M. Colangelo, S. W. Nam, and K. K. Berggren, *Phys. Rev. D* **106**, 112005 (2022), 2110.01586.
- [26] K. Agashe, Y. Cui, L. Necib, and J. Thaler, *JCAP* **10**, 062 (2014), 1405.7370.
- [27] J. Berger, Y. Cui, and Y. Zhao, *JCAP* **02**, 005 (2015), 1410.2246.
- [28] K. Kong, G. Mohlabeng, and J.-C. Park, *Phys. Lett. B* **743**, 256 (2015), 1411.6632.
- [29] J. F. Cherry, M. T. Frandsen, and I. M. Shoemaker, *Phys. Rev. Lett.* **114**, 231303 (2015), 1501.03166.
- [30] L. Necib, J. Moon, T. Wongjirad, and J. M. Conrad, *Phys. Rev. D* **95**, 075018 (2017), 1610.03486.
- [31] H. Alhazmi, K. Kong, G. Mohlabeng, and J.-C. Park, *JHEP* **04**, 158 (2017), 1611.09866.
- [32] D. Kim, J.-C. Park, and S. Shin, *Phys. Rev. Lett.* **119**, 161801 (2017), 1612.06867.
- [33] C. Kachulis et al. (Super-Kamiokande), *Phys. Rev. Lett.* **120**, 221301 (2018), 1711.05278.
- [34] G. F. Giudice, D. Kim, J.-C. Park, and S. Shin, *Phys. Lett. B* **780**, 543 (2018), 1712.07126.
- [35] A. Chatterjee, A. De Roeck, D. Kim, Z. G. Moghaddam, J.-C. Park, S. Shin, L. H. Whitehead, and J. Yu, *Phys. Rev. D* **98**, 075027 (2018), 1803.03264.
- [36] D. Kim, K. Kong, J.-C. Park, and S. Shin, *JHEP* **08**, 155 (2018), 1804.07302.
- [37] T. Bringmann and M. Pospelov, *Phys. Rev. Lett.* **122**, 171801 (2019), 1810.10543.
- [38] Y. Ema, F. Sala, and R. Sato, *Phys. Rev. Lett.* **122**, 181802 (2019), 1811.00520.
- [39] C. Ha et al. (COSINE-100), *Phys. Rev. Lett.* **122**, 131802 (2019), 1811.09344.
- [40] D. Kim, J.-C. Park, and S. Shin, *Phys. Rev. D* **100**, 035033 (2019), 1903.05087.
- [41] L. Heurtier, D. Kim, J.-C. Park, and S. Shin, *Phys. Rev. D* **100**, 055004 (2019), 1905.13223.
- [42] J. Berger, Y. Cui, M. Graham, L. Necib, G. Petrillo, D. Stocks, Y.-T. Tsai, and Y. Zhao, *Phys. Rev. D* **103**, 095012 (2021), 1912.05558.
- [43] D. Kim, P. A. N. Machado, J.-C. Park, and S. Shin, *JHEP* **07**, 057 (2020), 2003.07369.
- [44] A. De Roeck, D. Kim, Z. G. Moghaddam, J.-C. Park, S. Shin, and L. H. Whitehead, *JHEP* **11**, 043 (2020), 2005.08979.
- [45] Q.-H. Cao, R. Ding, and Q.-F. Xiang, *Chin. Phys. C* **45**, 045002 (2021), 2006.12767.
- [46] Y. Jho, J.-C. Park, S. C. Park, and P.-Y. Tseng, *Phys. Lett. B* **811**, 135863 (2020), 2006.13910.
- [47] H. Alhazmi, D. Kim, K. Kong, G. Mohlabeng, J.-C. Park, and S. Shin, *JHEP* **05**, 055 (2021), 2006.16252.
- [48] Y. Jho, J.-C. Park, S. C. Park, and P.-Y. Tseng (2021), 2101.11262.
- [49] W. Wang, L. Wu, W.-N. Yang, and B. Zhu, *Phys. Rev. D* **107**, 073002 (2023), 2111.04000.
- [50] J.-W. Wang, A. Granelli, and P. Ullio, *Phys. Rev. Lett.* **128**, 221104 (2022), 2111.13644.
- [51] X. Cui et al. (PandaX-II), *Phys. Rev. Lett.* **128**, 171801 (2022), 2112.08957.
- [52] R. Xu et al. (CDEX), *Phys. Rev. D* **106**, 052008 (2022), 2201.01704.
- [53] N. F. Bell, J. B. Dent, B. Dutta, S. Ghosh, J. Kumar, J. L. Newstead, and I. M. Shoemaker, *Phys. Rev. D* **104**, 076020 (2021), 2108.00583.
- [54] G. Adhikari et al. (COSINE-100), *Phys. Rev. Lett.* **131**, 21802 (2023), 2306.00322.
- [55] A. Kamada, H. J. Kim, J.-C. Park, and S. Shin, *JCAP* **10**, 052 (2022), 2111.06808.
- [56] J. H. Kim, K. Kong, S. H. Lim, and J.-C. Park (2024), in preparation.
- [57] D. Baumann, *Cosmology* (Cambridge University Press, 2022).
- [58] N. Becker, D. C. Hooper, F. Kahlhoefer, J. Lesgourgues, and N. Schöneberg, *Journal of Cosmology and Astroparticle Physics* **2021**, 019 (2021), URL <https://doi.org/10.1088/2F1475-7516/2F2021/2F02/2F019>.
- [59] D. Blas, J. Lesgourgues, and T. Tram, *JCAP* **07**, 034 (2011), 1104.2933.
- [60] N. Aghanim et al. (Planck), *Astron. Astrophys.* **641**, A6 (2020), [Erratum: *Astron. Astrophys.* 652, C4 (2021)], 1807.06209.
- [61] K.-Y. Choi, J.-O. Gong, and C. S. Shin, *Phys. Rev. Lett.* **115**, 211302 (2015), 1507.03871.
- [62] A. L. Erickcek, *Phys. Rev. D* **92**, 103505 (2015), 1504.03335.
- [63] V. Springel, *Monthly Notices of the Royal Astronomical Society* **364**, 1105 (2005), URL <https://doi.org/10.1111/2Fj.1365-2966.2005.09655.x>.
- [64] V. Springel, J. Wang, M. Vogelsberger, A. Ludlow, A. Jenkins, A. Helmi, J. F. Navarro, C. S. Frenk, and S. D. M. White, *Monthly Notices of the Royal Astronomical Society* **391**, 1685 (2008), URL <https://doi.org/10.1111/2Fj.1365-2966.2008.14066.x>.
- [65] M. Crocce, S. Pueblas, and R. Scoccimarro, *Monthly Notices of the Royal Astronomical Society* **373**, 369 (2006), URL <https://doi.org/10.1111/2Fj.1365-2966.2006.11040.x>.
- [66] S. Paduroiu, Y. Revaz, and D. Pfenniger, *Structure formation in warm dark matter cosmologies: Top-bottom upside-down* (2015), 1506.03789.
- [67] M. Leo, C. M. Baugh, B. Li, and S. Pascoli, *Journal of Cosmology and Astroparticle Physics* **2017**, 017 (2017), URL <https://doi.org/10.1088/2F1475-7516/2F2017/2F11/2F017>.
- [68] P. Bode, J. P. Ostriker, and N. Turok, *The Astrophysical Journal* **556**, 93 (2001), URL <https://doi.org/10.1086/2F321541>.
- [69] V. Springel, S. D. M. White, G. Tormen, and G. Kauffmann, *Mon. Not. Roy. Astron. Soc.* **328**, 726 (2001), astro-ph/0012055.
- [70] V. Springel, R. Pakmor, O. Zier, and M. Reinecke, *Monthly Notices of the Royal Astronomical Society* **506**, 2871 (2021), URL <https://doi.org/10.1093/2Fmnras/2F5tab1855>.
- [71] J. D. Simon and M. Geha, *The Astrophysical Journal* **670**, 313 (2007), URL <https://doi.org/10.1086/2F521816>.
- [72] A. Klypin, I. Karachentsev, D. Makarov, and O. Nasonova, *Monthly Notices of the Royal Astronomical Society* **454**, 1798 (2015), URL <https://doi.org/10.1093/2Fmnras/2F5tstv2040>.
- [73] M. R. Lovell, V. Gonzalez-Perez, S. Bose, A. Boyarsky, S. Cole, C. S. Frenk, and O. Ruchayskiy, *Mon. Not. Roy. Astron. Soc.* **468**, 2836 (2017), 1611.00005.
- [74] S. Y. Kim and A. H. G. Peter (2021), 2106.09050.
- [75] Y. Fukuda et al. (Super-Kamiokande), *Nucl. Instrum. Meth. A* **501**, 418 (2003).
- [76] E. Aprile et al. (XENON), *Eur. Phys. J. C* **77**, 881 (2017), 1708.07051.

- [77] A. Abusleme et al. (JUNO), Prog. Part. Nucl. Phys. **123**, 103927 (2022), 2104.02565.